In-situ Electrochemical Surface Plasmon Resonance Study on Lithium Underpotential Deposition and Stripping in Bis(fluorosulfonyl)amide-based Ionic Liquids

Shiwei Zhang, Takashi Yamazawa, Tetsuo Sakka, Naoya Nishi*

*E-mail: nishi.naoya.7e@kyoto-u.ac.jp

Department of Energy and Hydrocarbon Chemistry, Graduate School of Engineering,

Kyoto University, Kyoto 615-8510, Japan

Abstract:

To sensitively detect the electrode surface roughness change in the initial process of the lithium electrodeposition/dissolution processes in ionic liquids (ILs), electrochemical surface plasmon resonance (ESPR) measurements were performed in an in-situ manner on a gold electrode in a glyme-Li salt solvate IL, tetraglyme/lithium bis(fluorosulfonyl)amide ($[Li(G4)^+][FSA^-]$), and also an IL, 1-butyl-3-methylimidazolium bis(fluorosulfonyl)amide ($[C_4mim^+][FSA^-]$) containing 100 mM $Li^+[FSA^-]$. The SPR angle shifts ($\Delta\theta_{SPR}$) were tracked simultaneously with the repetitively recorded cyclic voltammograms (CVs) of the Li underpotential deposition (UPD)/underpotential stripping (UPS). $\Delta\theta_{SPR}$ increased/decreased in the UPD/UPS processes, sensitively responding to the refractive index change at the IL/electrode interface. The time derivative $\Delta\theta_{SPR}$ curves basically reproduced the CVs, but were significantly less influenced by residual current, indicating that ESPR is an effective in-situ method to track the Li UPD/UPS processes. In $[Li(G4)^+][FSA^-]$, the shift amounts of $\Delta\theta_{SPR}$ per deposited Li amount did not change as the CV scan was repeated, indicating no change in surface roughness. In contrast, in $[C_4mim^+][FSA^-]$, the same parameter increased with increasing the scan number, reflecting the increase in surface roughness as confirmed by Fresnel reflectivity simulations. The comparison of ESPR results with the simulations suggests that for both the two ILs the surface of the deposited Li layer is smoothed during the period after the Li UPD and before the Li UPS in CVs.

Introduction

Lithium metallic anode with a high energy density is attractive in the Li-metal batteries that are regarded as the next-generation Li-ion batteries.[1-3] In the charging process of Li-metal batteries, Li electrodeposition is a vital electrochemical process occurred on the metallic anode. As promising electrolytes for the Li-metal batteries,[4-7] ionic liquids (ILs) show the characteristics such as non-volatility, non-flammability, wide potential window, and high ionic conductivity. Therefore, the mechanisms of the Li^+ ion transport and Li^+ electrodeposition/dissolution processes in ILs are urgent to be clarified.

Compared to the conventional aqueous or organic electrolytes, ILs have a complex ionic structure and high ionic concentration, resulting in a peculiar solvation environment and a highly ordered structure on the electrode. Several experimental methods, such as electrochemical impedance spectroscopy,[8-10] in situ interferometry,[11] and nuclear magnetic resonance (NMR) spectroscopy,[8,12] were used to investigate the Li^+ ion transport process near the electrode, indicating that the low transport number of Li^+ ion in IL electrolytes can limit the discharging current due to the polarization in the IL electrolytes,[8,12] and that the change in ionic concentration near the electrode alters the local viscosity.[11] Scanning electron microscopy (SEM)[9-11,13,14] is a powerful method to visualize the electrode surface in an ex-situ manner after the Li electrodeposition process in ILs. As for the in-situ experimental methods to study Li electrodeposition in ILs, scanning tunneling microscopy (STM),[15] optical microscope observation,[13,16] atomic force microscopy (AFM),[17,18] and electrochemical quartz crystal microbalance (EQCM)[14,19] were used to study not only the electrode surface morphology[13-16] but also the IL structure on the electrode.[14,17-19]

The Li electrodeposition/dissolution processes induce the increase in surface roughness of the metal anode, which significantly affects the electrochemical performance of Li-ion batteries. The surface roughness increase can further lead to Li dendrite formation during the Li electrodeposition, which is a serious problem for the electrochemical reversibility, durability, and safety of Li-metal batteries.[20,21] The sensitive detection of the change in electrode surface roughness in the very initial stage of Li electrodeposition would be helpful to monitor and understand the initiation process of Li dendrite growth.[22-24] Therefore, in-situ measurement of tracking the change in the electrode surface roughness is desirable to investigate and understand the Li electrodeposition/dissolution process in the Li-metal batteries.

In the present study, electrochemical surface plasmon resonance (ESPR) is proposed as an in-situ method to sensitively detect the change in the metal electrode surface roughness during the Li deposition/dissolution processes. ESPR is an experimental method to track the change in refractive indices at the metal/electrolyte interface. Compared with the other in-situ methods (STM, AFM, optical imaging, and EQCM) described above, ESPR does not have any lateral resolution that STM and AFM beautifully attain on the angstrom order on single crystal electrodes. In contrast, the surface-normal resolution of ESPR is comparable to that for STM and AFM, on the angstrom order, which is significantly higher than that for EQCM and optical imaging, especially when focusing on the surface roughness. This high resolution of ESPR in the surface-normal direction is maintained even when we would like to focus on the surface roughness change of polycrystalline electrodes whose surface is already rough as is the case with the present study. Also, the detection principle of ESPR, the local refractive indices around the electrode surface, can be beneficial when focusing on the metal

electrodeposition, which leads to significant refractive index change compared with that caused by other phenomena, as we will discuss in Results and Discussion. For the IL side of the IL|electrode interface, ESPR has been used to study the dynamics in the electric double layer (EDL),[25,26] the diffusion layer formation,[27] and even ionic reorientation in the first ionic layer on the electrode[25,28] by tracking the SPR angle, which is the incident angle of light where the reflectivity is the lowest. On the other hand, for the metal electrode side of the IL|electrode interface, ESPR can be used to monitor the metal electrodeposition process. We demonstrated that the gold electrode smoothing can be detected on the order of Å as the decrease in the SPR angle shift by repetitive reductive deposition and oxidative dissolution of Cu in 1-butyl-3-methylimidazolium bis(trifluoromethanesulfonyl)amide ($[C_4mim^+][TFSA^-]$).[29] In the same IL, we also found that coumarin, a leveling additive, actually smooths the electrodeposited Co surface in the initial electrodeposition stage, whereas thiourea roughens the gold electrode surface underneath.[30] A few studies have also successfully applied ESPR to the bulk electrodeposition of Li in organic electrolytes. Jin et al.[31] performed plasmonic monitoring of the morphology evolution of Li metal deposited on Ag array electrodes and identified two different deposition pathways, ideal and nonideal ones, under different conditions, the latter of which triggers the Li dendrite formation. Kitta et al.[32] compared the SPR reflectance spectra during the Li electrodeposition on a Cu electrode with the simulation results of Li morphology models, and revealed that a model with the isotropic nucleus growth can explain the experimental spectra.

In the present study, we study the Li underpotential deposition (UPD)/underpotential stripping (UPS) processes on a gold electrode to focus on the very initial process of Li electrodeposition and the concomitant change in the electrode surface

roughness by tracking the SPR angle. As the electrolyte, we choose two ILs based on bis(fluorosulfonyl)amide (FSA^-), which has been recognized as a key component for the IL application to Li-ion batteries.[33-37] One is tetraglyme/lithium bis(fluorosulfonyl)amide ($[Li(G4)^+][FSA^-]$), which is one of glyme-Li salt solvate ILs that are promising electrolytes for Li-metal batteries, owing to the high transport number of Li^+,[12,38-41] as well as high thermal stability and a wide electrochemical window like typical ILs.[12] In the G4 based solvate ILs, the complex formation of Li^+ with G4 endows the thermal/electrochemical stability of G4 and high ionic conductivity at the same time to the solvate ILs.[12,38-40] We also investigate an FSA-based IL, $[C_4mim^+][FSA^-]$ containing 100 mM $Li^+[FSA^-]$. Combining with the quantitative simulation analysis of SPR angle shift, we demonstrated that the roughness of gold surface does not change during the repetitive deposition and dissolution of Li in $[Li(G4)^+][FSA^-]$, whereas the gold electrode surface is gradually roughened in $[C_4mim^+][FSA^-]$. For both the two ILs, the surface of the deposited Li layer is found to be smoothed during the period after the Li UPD and before the Li UPS.

Experimental

$[Li(G4)^+][FSA^-]$ was prepared as an equimolar mixture of G4 (Tokyo Chemical Industry) with $Li^+[FSA^-]$ (Tokyo Chemical Industry). $[C_4mim^+][FSA^-]$ was prepared from $[C_4mim^+]Cl^-$ (synthesized) and $Li^+[FSA^-]$ and purified as the same procedure for $[C_4mim^+][TFSA^-]$ as in our previous studies.[26-30] The refractive indices of the ILs were measured at 656 nm by the multi-wavelength Abbe refractometer (DR-M2, Atago): 1.425 for $[Li(G4)^+][FSA^-]$ and 1.449 for $[C_4mim^+][FSA^-]$ containing 100 mM $Li^+[FSA^-]$, and were approximately used for the simulation (details shown below) at 670 nm.

The ESPR measurements were performed, as the same manner as our previous work,[25-30] using an SPR instrument (Springle, Kinetic Evaluation Instruments) with a Kretschmann configuration,[42] in which the SPR was induced by a 670-nm laser illuminating an IL-covered gold film on a prism. A three-electrode electrochemical cell was set up with the gold film (thickness d_{film} = 50 nm, refractive index n^*_{Au}= 0.096 + 3.69I at 670 nm)[43] deposited on a SF15 glass (refractive index n_{prism} = 1.691 at 670 nm) as the working electrode, a Pt wire as the counter electrode, and an AgCl coated Ag wire as the quasi-reference electrode. Before the measurement, the gold film surface was cleaned in a piranha solution for at least 2 h. After 12 h vacuum evacuation, the ILs were injected into the cell to cover the gold surface (area: 7.1×10^{-2} cm^2). Above the ILs, the atmosphere of Ar gas (99.9%) was kept over the whole measurement. In the simultaneous cyclic voltammetry and ESPR measurement, a PC-controlled potentiostat (Autolab Type III) controlled the potential of the working electrode vs. Ag/AgCl, E, with the scan rate of 50 mV s^{-1}, which is in the range of 10~100 mV s^{-1} adopted in previous CV studies on Li UPD.[18,44-46] Before each scan, E was held at −2 V for 1000 s to stabilize the SPR angle and current.

Model

To analyze the experimental results, the Fresnel reflectivity simulations of SPR angle were performed. In the model, the roughness of gold surface is modeled as the thickness of a mixture layer, consisting of Au, Li, and IL, as our previous ESPR work on the Co electrodeposition.[30] For the Au surface without Li layer deposited on it, shown in Figure 1a, the surface roughness, Δd_{Au}, is regarded as the thickness of a mixture layer consisting of Au and IL, Δd_{mix1}, and hence $\Delta d_{mix1} = \Delta d_{Au}$. The thickness of the Au layer

in the model, $d_{film'}$, is expressed as $d_{film'} = d_{film} - \Delta d_{Au}/2$, where $d_{film} = 50$ nm is the effective thickness of the Au film. It should be noted that the surface roughness detectable with ESPR is limited to "local" one that has a lateral scale shorter than the optical wavelength. When Li UPD layer is electrodeposited on the Au film (Figure 1b), the mixture layer consists of Au, Li, and IL. To take into account the surface roughness difference between the deposited Li UPD layer surface and the Au electrode surface, we assume that the deposited Li UPD layer has two different thickness on the peak, $d_{Li\text{-}p}$, and on the valley, $d_{Li\text{-}v}$, as shown in Figure 1c. The effective thicknesses of Li UPD layer is $d_{Li} = (d_{Li\text{-}p} + d_{Li\text{-}v}) / 2$, and the thickness of the mixture layer after Li deposition increases to $\Delta d_{mix2} = \Delta d_{Au} + d_{Li\text{-}p}$.

Using Fresnel equations,[47] we can express the reflectivity, R, at the prism|Au|IL (Figure 1a) or prism|Au|Li|IL (Figure 1b) interface by using the following equations:

$$n_i \sin\theta_i = n_{prism} \sin\theta_{prism} \tag{1}$$

$$q_i = \frac{\cos\theta_i}{n_i} \tag{2}$$

$$\beta_i = \frac{2\pi}{\lambda} n_i d_i \cos\theta_i \tag{3}$$

$$M_i = \begin{pmatrix} \cos\beta_i & -\mathrm{I}\, q_i^{-1} \sin\beta_i \\ -\mathrm{I}\, q_i \sin\beta_i & \cos\beta_i \end{pmatrix} \tag{4}$$

$$M = \prod_i M_i \tag{5}$$

$$R = \left| \frac{(M^{11} + M^{12} q_{IL}) q_{prism} - (M^{21} + M^{22} q_{IL})}{(M^{11} + M^{12} q_{IL}) q_{prism} + (M^{21} + M^{22} q_{IL})} \right|^2 \tag{6}$$

where λ is the wavelength and i is either of the layers (Au or mixture). n_i, θ_i, and d_i are the refractive index, the laser light angle with respect to the surface normal, and the thickness for the layer i, respectively. M^{ab} is the element at the a-th row and b-th column of the matrix M.

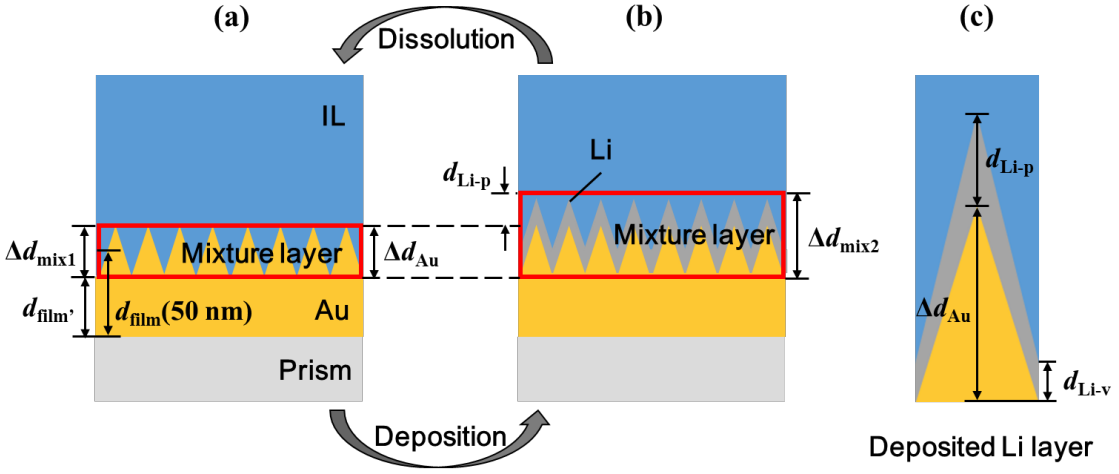

Figure 1. Simulation model with the mixture layer to represent the roughness of electrode surface **(a)** without and **(b)** with the Li deposited layer. **(c)** Model of the deposited Li layer on the electrode surface.

According to the Bruggeman effective medium approximation,[48] the refractive index of the mixture layer, n_{mix}, can be written as:

$$\sum_j f_j \frac{{n_j}^2 - {n_{mix}}^2}{{n_j}^2 + 2{n_{mix}}^2} = 0 \quad (7)$$

where f_j is the fraction of j, either of Au, Li, and IL, in the mixture layer. We assumed that the areal fraction of j in the mixture layer in Figure 1 corresponds to f_j; in Figure 1a, $f_{Au} = f_{IL} = 0.5$, and in Figure 1b,c, $f_{Li} = (d_{Li\text{-}p} + d_{Li\text{-}v}) / 2 (d_{Li\text{-}p} + \Delta d_{Au})$, $f_{Au} = \Delta d_{Au} / 2 (d_{Li\text{-}p} + \Delta d_{Au})$, $f_{IL} = (\Delta d_{Au} + d_{Li\text{-}p} - d_{Li\text{-}v}) / 2 (d_{Li\text{-}p} + \Delta d_{Au})$.[30]

In the simulations, Δd_{Au}, $d_{Li\text{-}p}$, and $d_{Li\text{-}v}$ are the three independent variables. At various values of these three variables, we calculated the reflectivity R as a function of θ_{prism} and then obtained the SPR angle, θ_{SPR}, where R is the minimum. Then we obtained $\Delta\theta_{SPR}$ accompanied by the UPD/UPS processes to compare with the ESPR experimental results.

Results and Discussion

Figure 2 shows the CVs (a, b) and SPR angle shifts (c, d), $\Delta\theta_{SPR}$, during the UPD/UPS process for the two ILs. For each IL, all the potential scans of 8 cycles were started from −2 V to the negative direction. For $[Li(G4)^+][FSA^-]$, the scan range was from −3 V to −1.8 V, while for $[C_4mim^+][FSA^-]$, it was from −2.8 V to −1.5 V, because for the latter the UPD/UPS peaks were 0.2 V more positive (see the discussion below). In each CV, a current peak pair assignable to the Li UPD/UPS was observed as previous studies of Li UPD/UPS in organic electrolytes[44,45] and ILs[18,46] on gold. For the solvate IL, $[Li(G4)^+][FSA^-]$, the reductive deposition peak of Li UPD appeared at −2.9 V in the negative-going scan, just before the bulk Li deposition starts. In the positive-going scan,

the oxidation dissolution peak of Li UPS appeared at −2.2 V. The peak positions and peak separation are similar to those previously reported.[44,45] For [C_4mim$^+$][FSA$^-$], the corresponding peak potentials are −2.7 V and −2.0 V. The peak potentials for [C_4mim$^+$][FSA$^-$] are about 0.2 V more positive than the counterparts for the glyme solvate IL, implying that Li^+ ions in the latter are thermodynamically more stable.

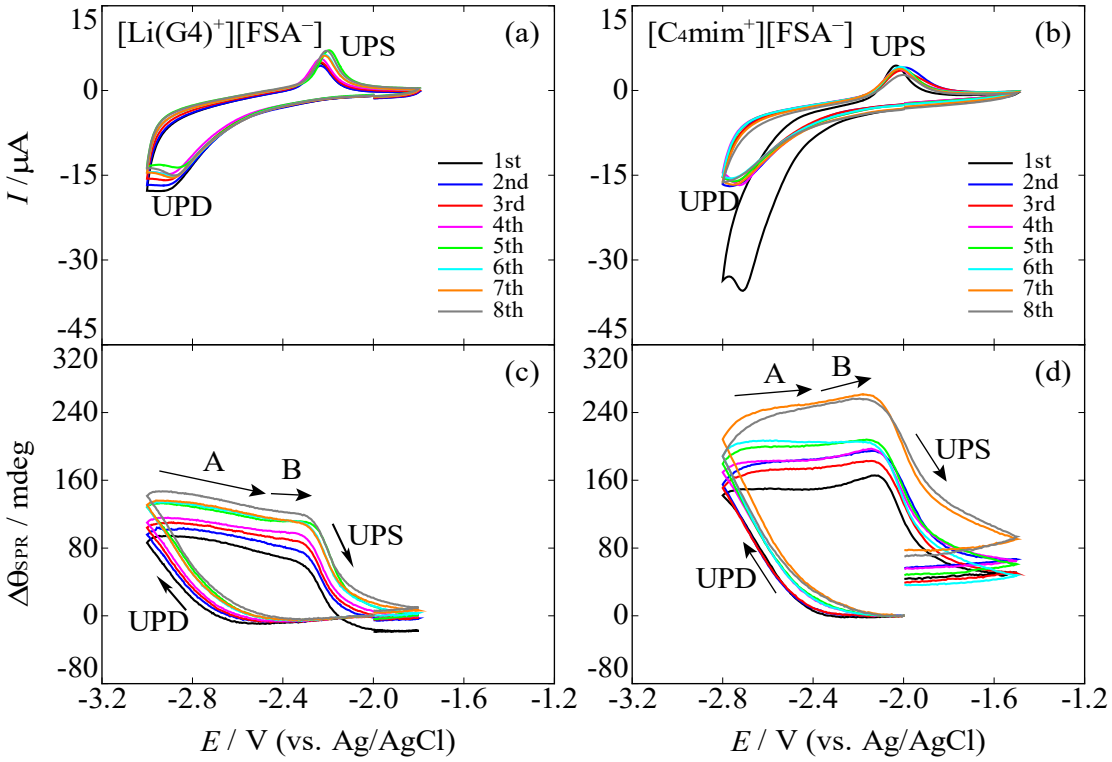

Figure 2. **(a, b)** CVs and **(c, d)** SPR angle shifts during the repetitive Li UPD/UPS processes of 8 scan cycles at the scan rate of 50 mV/s in **(a, c)** [Li(G4)$^+$][FSA$^-$] and **(b, d)** [C_4mim$^+$][FSA$^-$] containing 100 mM Li^+[FSA$^-$].

$\Delta\theta_{SPR}$ is sensitive enough to respond to the interfacial refractive indices change due to the Li UPD/UPS processes; corresponding to the reduction peak (Li UPD) and oxidation peak (Li UPS) in CVs, an increase and decrease in $\Delta\theta_{SPR}$, respectively, can be seen in Figure 2c,d. Similar $\Delta\theta_{SPR}$ behaviors were reported in previous ESPR studies on Cu[29] and Co[30] electrodeposition, in which $\Delta\theta_{SPR}$ was correlated with the deposited amount of Cu and Co. Besides, it was demonstrated that $\Delta\theta_{SPR}$ also changes with the surface roughness of the electrode[29,30] and the deposited layer.[30] $\Delta\theta_{SPR}$ shows different behaviors in $[Li(G4)^+][FSA^-]$ and $[C_4mim^+][FSA^-]$ in the positive-going scan after the Li UPD and before UPS processes (Figure 2c,d). In $[Li(G4)^+][FSA^-]$, $\Delta\theta_{SPR}$ decreases after the Li UPD (process A in Figure 2c), while it tends to be flat (process B in Figure 2c) in the very beginning of the Li UPS. The same $\Delta\theta_{SPR}$ behavior, as well as the response to the UPD/UPS, has also been found in another G4 solvate IL, $[Li(G4)^+][TFSA^-]$ (see Figure S1). In contrast, in $[C_4mim^+][FSA^-]$ (Figure 2d), the slope is more positive overall; $\Delta\theta_{SPR}$ is flat in the process A and then increases in the next process B. The slope increase is ascribable to the roughness increase in the gold electrode surface, as discussed below.

During the scan cycles, $\Delta\theta_{SPR}$ varies with the deposited Li amount and the surface roughness of the Au electrode, which can be written as:[29]

$$\Delta\theta_{SPR} = \alpha\, d_{Li} + \beta \Delta d_{Au} \qquad (8)$$

where the two coefficients, α and β, are both positive and constants for small d_{Li} and Δd_{Au}. It should be noted that $\Delta\theta_{SPR}$ is also affected by the surface roughness of the deposited Li layer, Δd_{Li} (= $d_{Li\text{-}p} - d_{Li\text{-}v}$), however, the sensitivity of $\Delta\theta_{SPR}$ towards Δd_{Au} is higher than that towards Δd_{Li} (see the discussion in Figure 5 below). Besides, $\Delta\theta_{SPR}$ is also generally sensitive enough to the ionic concentration in the EDL[25,26,28] and the diffusion layer,[27,29]

but this is not the case with the present Li UPD/UPS case. For the former, the Li UPD/UPS potentials are far negative from the potential of zero charge (PZC), where the EDL structure is in the "crowding" state and the first ionic layer is saturated with cations, therefore the contribution of EDL structure is small to be neglected here.[26,49] For the latter, i.e., the contribution of diffusion layer, the deposited/stripped Li amount is small with only about monatomic layer thickness, and in contrast, the concentration of Li^+ in the ILs is high enough to be regarded as constant during the Li UPD/UPS. The time derivative of $\Delta\theta_{SPR}$ can be expressed as:

$$\frac{d\Delta\theta_{SPR}}{dt} = -\frac{\alpha V_{Li}}{F} i_{Li} + \beta \frac{d\Delta d_{Au}}{dt} \quad (9)$$

where V_{Li} is the molar volume of Li metal, F is the Faraday constant, and i_{Li} is the current density for the Li UPD/UPS processes. This is because $i_{Li} = -dq_{Li}/dt = -(F/V_{Li})\, dd_{Li}/dt$, where q_{Li} is the surface charge density for the Li UPD layer. Here, V_{Li} is evaluated to be 13.0 $cm^3 \cdot mol^{-1}$ by the molar mass of Li, 6.941 $g \cdot mol^{-1}$, and the density of Li metal at room temperature, 0.534 $g \cdot cm^{-3}$. Therefore, the time derivative of SPR angle is in a linear relationship to the current in the Li UPD/UPS processes with the contribution of surface roughness change.

The time derivative $\Delta\theta_{SPR}$ curves are shown in Figure 3. One can see that the curves basically reproduce the behaviors in the CVs in Figure 2, including the redox peak pair. The Li UPD/UPS processes are reflected in the time derivative $\Delta\theta_{SPR}$ curves, but less influenced by residual current, because n_{Li} is significantly different from n_{IL} than other organic/inorganic compounds that may be produced via residual current. Especially, a large reduction current in the 1st cycle in [C_4mim^+][FSA^-] (Figure 2b), which is likely due to the reductive decomposition of IL ions, has no effect on the corresponding time derivative $\Delta\theta_{SPR}$ (Figure 3b). This demonstrates that ESPR is selectively sensitive

to the Li electrodeposition/dissolution process.

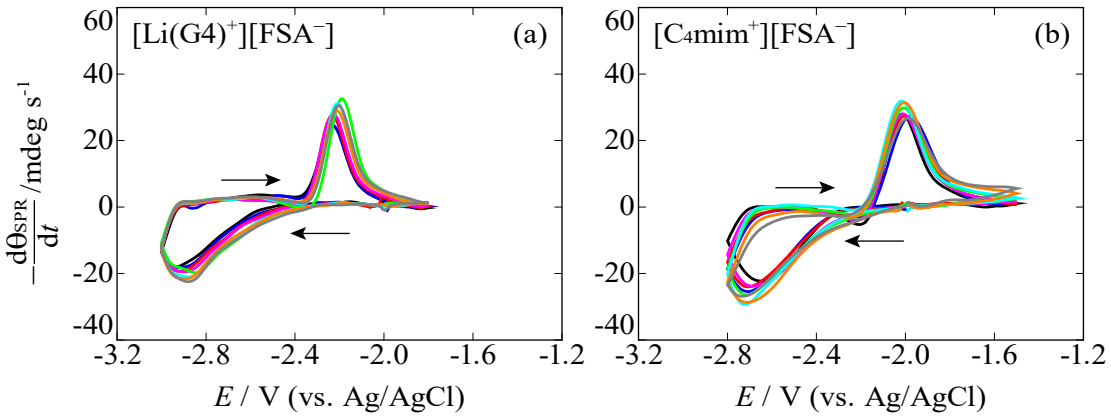

Figure 3. Time derivative of SPR angle during Li UPD/UPS processes in **(a)** $[Li(G4)^+][FSA^-]$ and **(b)** $[C_4mim^+][FSA^-]$ containing 100 mM $Li^+[FSA^-]$, obtained from Figure 2c,d. The line colors correspond to those in Figure 2.

$\Delta\theta_{SPR}$ is sensitive to both the amount of deposited Li and the surface roughness (eq 8). In the last paragraph, we investigated the former contribution as the UPD/UPS current (eq 9). In the following, to extract the contribution of the latter, i.e., the surface roughness, we normalized $\Delta\theta_{SPR}$ with q_{Li} as follows:

$$\kappa \equiv \frac{\Delta\theta_{SPR}}{q_{Li}} = \alpha \frac{V_{Li}}{F} + \frac{\beta \Delta d_{Au}}{q_{Li}} \tag{10}$$

The change in surface roughness and $\Delta\theta_{SPR}$, both normalized with q_{Li}, are in a linear relationship with the constant $\alpha V_{Li}/F$ term. Here, we define the absolute value for the increase in $\Delta\theta_{SPR}$ during Li UPD as $\Delta\theta_R$, and that for the decrease during Li UPS as $\Delta\theta_O$, which were evaluated by the $\Delta\theta_{SPR}$ difference between before and after the Li UPD and UPS processes, respectively. q_{Li} was evaluated by the integration of the oxidation

current peak of the CVs in Figure 2. The details on their evaluation methods and results are shown in Figures S2 and S3, respectively.

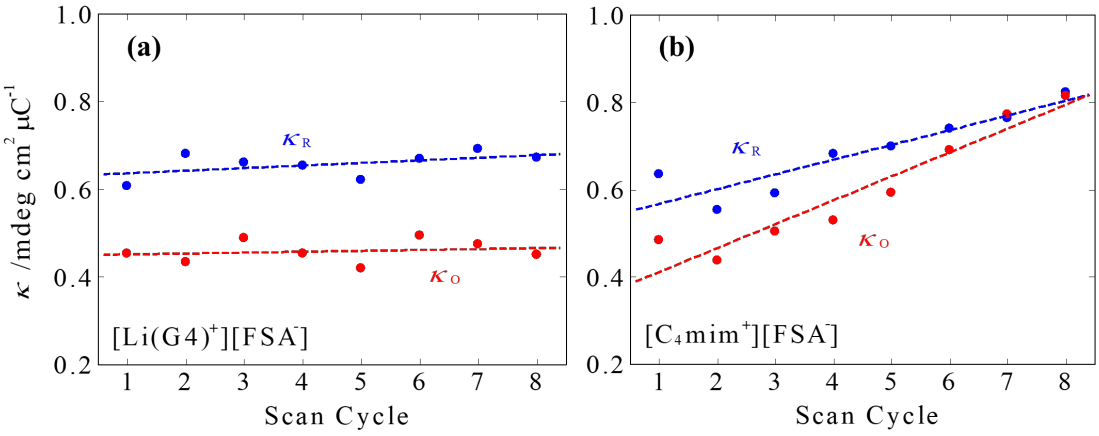

Figure 4. Scan cycle number dependence of κ_R (blue points) and κ_O (red points), which are the absolute values of the change in $\Delta\theta_{SPR}$ during the UPD and UPS, respectively, divided by the surface charge density for the Li deposition layer, q_{Li}, for **(a)** [Li(G4)$^+$][FSA$^-$] and **(b)** [C$_4$mim$^+$][FSA$^-$] containing 100 mM Li$^+$[FSA$^-$]. The dashed lines are from linear least-squares regressions.

The shift values of $\Delta\theta_R$ and $\Delta\theta_O$ normalized with q_{Li}, defined as κ_R and κ_O, respectively, are shown in Figure 4. For [Li(G4)$^+$][FSA$^-$] in Figure 4a, κ_R and κ_O are nearly constant in the 8 scan cycles, indicating that the surface roughness does not change during the repetitive Li UPD/UPS processes. In contrast, for [C$_4$mim$^+$][FSA$^-$] shown in Figure 4b, κ_R and κ_O increase together with increasing the scan cycle, indicating that the surface roughness increases with the repetitive Li UPD/UPS processes (see Figure S4 for the simulation results). This contrasting surface roughness results for these two ILs, i.e., no change for the former and increase for the latter, were reproduced with ex-situ AFM measurements where AFM images were taken before and after the ESPR measurements

for the 8-cycle UPD/UPS of Li (Figure S5). One can see that κ_R always has a larger value than κ_O, especially for [Li(G4)$^+$][FSA$^-$] in Figure 4a. For both the ILs, UPS takes a wider potential range than UPD (see Figures 2 and 3), hence the $\Delta\theta_R$ is relatively more affected by other factors, such as the potential dependence of ionic concentration in the EDL, when it is evaluated. Moreover, the roughness change in the Li layer surface after the Li UPD and before the Li UPS causes the difference between κ_R and κ_O; κ_O can be smaller than κ_R because of the surface smoothing, which is the case with [Li(G4)$^+$][FSA$^-$] (see the discussion for Figure 5 below).

In Figure 2, between the Li UPD and UPS in the two ILs, $\Delta\theta_{SPR}$ shows different trends, during the processes A and B. Since there is no change in the deposited Li amount during this period, these $\Delta\theta_{SPR}$ trends should reflect the surface roughness change, Δd_{Au} and Δd_{Li} (= $d_{Li\text{-}p} - d_{Li\text{-}v}$, see Figure 1c for definition). We introduce Δd_{Li} to analyze the $\Delta\theta_{SPR}$ in the processes A and B, by adding an additional term to eq 8 as follows:

$$\Delta\theta_{SPR} = \alpha\, d_{Li} + \beta\Delta d_{Au} + \gamma\Delta d_{Li} \qquad (11)$$

where γ is a positive constant that is smaller than β. Δd_{Li} indicates the roughness of the deposited Li layer surface beyond that of the gold surface underneath. We performed the simulation with variable Δd_{Au} and Δd_{Li} but constant d_{Li}. d_{Li} was fixed to be 0.29 nm, the thickness of the closely packed Li monolayer.[50] In the repetitive Li UPD/UPS scan cycles, the evaluated q_{Li} values are around 200 μC·cm^{-2} (Figure S3a,b), corresponding to the amount of monolayer deposition.[46,51,52] The simulation results are shown as 2-D density plots in Figure 5. One can see that the contour lines are close to vertical, which means $\gamma << \beta$ in eq 11. Before ESPR experiments, the surface roughness of the gold electrode, Δd_{Au}, was measured to be 1.1 nm by AFM.[30] Immediately after the Li UPD,

the deposited surface is likely rougher than the electrode surface, meaning $\Delta d_{Li} > 0$, although we have no clue to know the exact Δd_{Li} value. Here, we set the point at (Δd_{Au}, Δd_{Li}) = (1.1 nm, 0.1 nm) in the 2-D plots as the reference point that represents the surface condition after the Li UPD and before the process A in the CV scans.

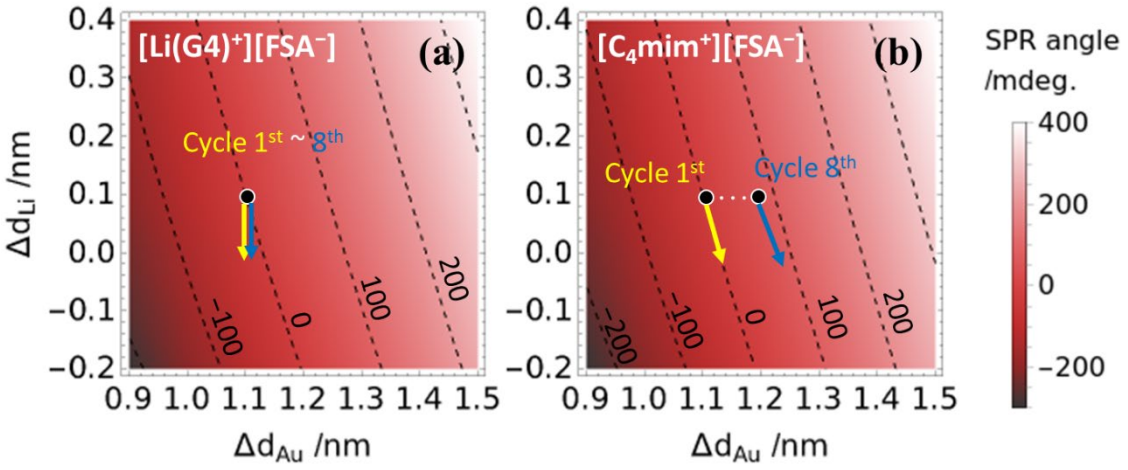

Figure 5. 2-D plots of $\Delta\theta_{SPR}$ against Δd_{Au} and Δd_{Li} for **(a)** [Li(G4)$^+$][FSA$^-$] and **(b)** [C$_4$mim$^+$][FSA$^-$] containing 100 mM Li$^+$[FSA$^-$]. The arrows indicate the possible direction of the surface roughness after the Li UPD and before the UPS (process A).

In Figure 5, the black points represent the status of Δd_{Au} and Δd_{Li} just after the Li UPD. As described above at Figure 2, in [Li(G4)$^+$][FSA$^-$], $\Delta\theta_{SPR}$ decreases after the Li UPD (process A) and then tends to be flat in the very beginning of the Li UPS (process B), while in [C$_4$mim$^+$][FSA$^-$], $\Delta\theta_{SPR}$ is flat or slightly increases after the Li UPD and then increases more obviously in the very beginning of the Li UPS. Also, Figure 4 has demonstrated the trends in Δd_{Au} after the scan cycles in the two ILs; for [Li(G4)$^+$][FSA$^-$], Δd_{Au} is not changed after the scan cycles of Li UPD/UPS processes, while Δd_{Au} increases for [C$_4$mim$^+$][FSA$^-$]. Taking into account these trends in $\Delta\theta_{SPR}$ in the process A and in

Δd_{Au} during the whole scan cycle, we can draw possible behaviors of the surface roughness condition as the arrows in Figure 5. For $[Li(G4)^+][FSA^-]$, after the Li UPD process, the deposited surface tends to be smooth, i.e., Δd_{Li} decreases, and the surface roughness of the Au electrode, Δd_{Au}, is constant, therefore $\Delta\theta_{SPR}$ decreases in the process A (Figures 5a and 2c). For $[C_4mim^+][FSA^-]$ (Figure 5b), the smoothing of the deposited surface is also effective, while Δd_{Au} tends to increase simultaneously, resulting in the flat $\Delta\theta_{SPR}$ for the early cycles in Figure 2d. As the scan cycle increases, we can see the increase in $\Delta\theta_{SPR}$ of the process A in Figure 2d, the increase in Δd_{Au} is likely to be more and more significant (Figure 5b). The increase in Δd_{Au} for $[C_4mim^+][FSA^-]$ is not surprising. Au-Li alloying/de-alloying is well-known during the electrodeposition/electrostripping of Li on the Au electrode, which roughens the Au surface or even produces a nanoporous Au surface layer.[53,54] For example, Gasparotto et al.[54] revealed by in-situ STM measurements that a number of monoatomically deep pits appear on the Au(111) after Li UPS in 1-butyl-1-methylpyrrolidinium $TFSA^-$, which is an IL whose ionic structures resemble C_4mim^+ and FSA^-. Rather, what is surprising is no change in Δd_{Au} for $[Li(G4)^+][FSA^-]$ (Figures 4 and 5), which is beneficial for the application of this salt to Li-metal batteries. As will be briefly discussed in the next paragraph, one of the reasons causing the difference is probably the EDL structure.

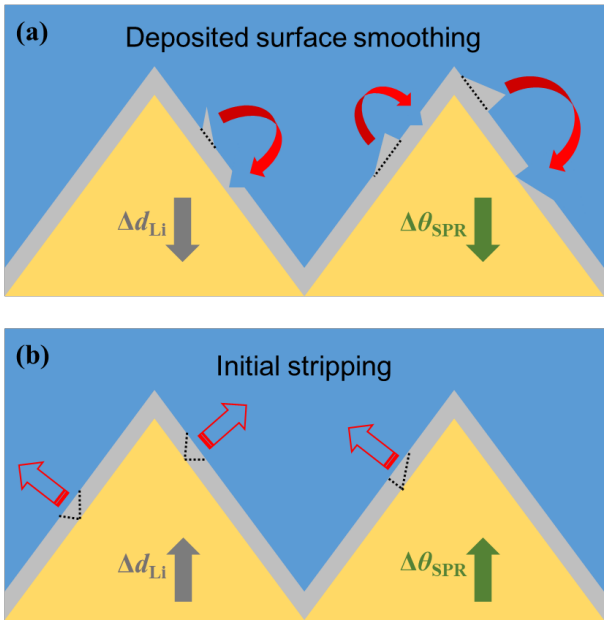

Figure 6. Schematic diagrams of **(a)** the deposited surface smoothing in the process A and **(b)** the "initial stripping" in the process B.

Based on all the investigation and analysis above, we propose a plausible mechanism for the two processes A and B as shown in Figure 6. As the discussion in Figure 5 above, the process A is ascribable to the deposited surface smoothing after the Li UPD (Figure 6a). This process, the Li surface diffusion, is driven to decrease the surface energy of the Li layer just after the Li UPD to make the surface more locally flat. In the process B, i.e., in the very beginning of Li UPS, the slope of $\Delta\theta_{SPR}$ is more positive than that in the process A (Figure 2c,d). This can be explained with "initial stripping" in which a small amount of Li is stripped from the deposited layer, causing an increase in surface roughness of the deposited layer. Only in the initial stripping stage $\Delta\theta_{SPR}$ increases, because in the later stage, the d_{Li} decrease, the negative contribution to $\Delta\theta_{SPR,}$ surpasses. The different behaviors in the process A between the two ILs are likely to originate from the EDL structure formed by the different solvate environments of Li^+. In glyme-Li solvate ILs, Li^+ can form a stable complex cation with glyme in bulk,[12,38-40]

but partial desolvation of the complex cation was suggested near the negatively charged electrode by experiments[55] and simulations.[56] Similarly, in FSA-based typical ILs, Li^+ tends to be partially desolvated in the EDL near the electrode surface.[57,58] However, the Li^+ ions still have different solvate environments in the EDL of the two ILs, with neutral G4 molecules for the former and with FSA^- anions for the latter. This can affect the Li^+ activity and thereby the Li electrodeposition process on the electrode, presumably resulting in the increase in Δd_{Au} only for $[C_4mim^+][FSA^-]$ but not for $[Li(G4)^+][FSA^-]$.

Conclusion

By using ESPR as an in-situ measurement, the Li UPD/UPS processes on the gold electrode in a glyme solvate IL and a typical IL were analyzed and compared. The time derivative SPR curves showed the same trends as CVs, but without the effects of residual current, indicating that ESPR is an effective in-situ method to track the metal electrodeposition/dissolution processes. Compared with the results of a model simulation, the roughness of the gold electrode surface was found to increase with the scan number in $[C_4mim^+][FSA^-]$ but not in $[Li(G4)^+][FSA^-]$. Moreover, the surface of the deposited Li layer was demonstrated to be smoothed between the Li UPD and UPS processes. Following the smoothing process, an initial stripping process was detected, which roughens the deposited Li surface in the very beginning of Li UPS. The present study proposes that $[Li(G4)^+][FSA^-]$ is an adequate electrolyte for Li-metal batteries, however, the investigation on various kinds of FSA-based ILs and other types is necessary, which will provide us with insight into the Li electrodeposition process in ILs.

Supporting Information

CVs, SPR angle shifts, and the time derivative of SPR angle shifts during the Li UPD/UPS in $[Li(G4)^+][TFSA^-]$; methods to evaluate κ_R, κ_O, and q_{Li}, and their values; simulation results of κ as a function of Δd_{Au}; ex-situ AFM images before and after ESPR measurements.

Acknowledgements

This work was partly supported by JSPS KAKENHI (No. 21H02046) and Izumi Science and Technology Foundation (2020-J-071). We acknowledge Dr. Yuki Kitazumi for the AFM measurements.

References

[1] J.-S. Lee, S. Tai Kim, R. Cao, N.-S. Choi, M. Liu, K. T. Lee, J Cho, Metal–air batteries with high energy density: Li–air versus Zn–air, *Adv. Energy Mater.* **1**, 34 (2011).

[2] W. Xu, J. Wang, F. Ding, X. Chen, E. Nasybulin, Y. Zhang, J. G. Zhang, Lithium metal anodes for rechargeable batteries, *Energy Environ. Sci.* **7**, 513 (2014).

[3] X.-Q. Zhang, X.-B. Cheng, Q. Zhang, Advances in interfaces between Li metal anode and electrolyte, *Adv. Mater. Interfaces* **5**, 1701097 (2018).

[4] L. X. Yuan, J. K. Feng, X. P. Ai, Y. L. Cao, S. L. Chen, H. X. Yang, Improved dischargeability and reversibility of sulfur cathode in a novel ionic liquid electrolyte, *Electrochem. Commun.* **8**, 610 (2006).

[5] C. J. Allen, S. Mukerjee, E. J. Plichta, M. A. Hendrickson, K. M. Abraham, Oxygen electrode rechargeability in an ionic liquid for the Li-air battery, *J. Phys. Chem. Lett.* **2**, 2420 (2011).

[6] S. Higashi, Y. Kato, K. Takechi, H. Nakamoto, F. Mizuno, H. Nishikoori, H. Iba, T. Asaoka, Evaluation and analysis of Li-air battery using ether-functionalized ionic liquid, *J. Power Sources* **240**, 14 (2013).

[7] L. Wang, H. R. Byon, *N*-Methyl-*N*-propylpiperidinium bis(trifluoromethanesulfonyl)imide-based organic electrolyte for high performance lithium–sulfur batteries, *J. Power Sources* **236**, 207 (2013).

[8] K. Yoshida, M. Tsuchiya, N. Tachikawa, K. Dokko, M. Watanabe, Correlation between battery performance and lithium ion diffusion in glyme–lithium bis(trifluoromethanesulfonyl)amide equimolar complexes, *J. Electrochem. Soc.* **159**, A1005 (2012).

[9] H. Sano, M. Kitta, M. Shikano, H. Matsumoto, Effect of temperature on Li electrodeposition behavior in room-temperature ionic liquids comprising quaternary ammonium cation, *J. Electrochem. Soc.* **166**, A2973 (2019).

[10] R. Furuya, T. Hara, T. Fukunaga, K. Kawakami, N. Serizawa, Y. Katayama, Deposition and dissolution of lithium in 1-methyl-1-methoxyethylpyrrolidinium bis(fluorosulfonyl)amide ionic liquid electrolyte with different compositions, *J. Electrochem. Soc.* **168**, 100516 (2021).

[11] A. Miki, K. Nishikawa, G. Kamesui, H. Matsushima, M. Ueda, M. Rosso, In situ interferometry study of ionic mass transfer phenomenon during the electrodeposition and dissolution of Li metal in solvate ionic liquids, *J. Mater. Chem. A* **9**, 14700 (2021).

[12] K. Ueno, K. Yoshida, M. Tsuchiya, N. Tachikawa, K. Dokko, M. Watanabe, Glyme–lithium salt equimolar molten mixtures: concentrated solutions or solvate ionic liquids?, *J. Phys. Chem. B* **116**, 11323 (2012).

[13] H. Sano, H. Sakaebe, H. Matsumoto, Observation of electrodeposited lithium by optical microscope in room temperature ionic liquid-based electrolyte, *J. Power Sources* **196**, 6663 (2011).

[14] G. Vanhoutte, N. R. Brooks, S. Schaltin, B. Opperdoes, L. van Meervelt, J.-P. Locquet, P. M. Vereecken, J. Fransaer, K. Binnemans, Electrodeposition of lithium from lithium-containing solvate ionic liquids, *J. Phys. Chem. C* **118**, 20152 (2014).

[15] L. H. S. Gasparotto, N. Borisenko, N. Bocchi, S. Zein El Abedin, F. Endres, In situ STM investigation of the lithium underpotential deposition on Au(111) in the air- and water-stable ionic liquid 1-butyl-1-methylpyrrolidinium bis(trifluoromethylsulfonyl)amide, *Phys. Chem. Chem. Phys.* **11**, 11140 (2009).

[16] H. Sano, H. Sakaebe, H. Matsumoto, In-situ optical microscope morphology observation of lithium electrodeposited in room temperature ionic liquids containing aliphatic quaternary ammonium cation, *Electrochemistry* **80**, 777 (2012).

[17] T. Carstens, A. Lahiri, N. Borisenko, F. Endres, $[Py_{1,4}]$FSI-NaFSI-based ionic liquid electrolyte for sodium batteries: Na^+ solvation and interfacial nanostructure on Au(111), *J. Phys. Chem. C* **120**, 14736 (2016).

[18] S. Liu, T. Cui, T. Carstens, J. Zhao, N. Borisenko, X. Liu, Z. Liu, Y. Li, F. Endres, In situ atomic force microscopic studies of LiFSI-$[Py_{1,4}]$FSI interfacial nanostructure on Au(111): solid electrolyte interphase and lithium underpotential deposition, *J. Phys. Chem. C* **125**, 27140 (2021).

[19] N. Serizawa, S. Seki, K. Takei, H. Miyashiro, K. Yoshida, K. Ueno, N. Tachikawa, K. Dokko, Y. Katayama, M. Watanabe, T. Miura, EQCM measurement of deposition and dissolution of lithium in glyme-Li salt molten complex, *J. Electrochem. Soc.* **160**, A1529 (2013).

[20] S. Li, M. Jiang, Y. Xie, H. Xu, J. Jia, J. Li, Developing high-performance lithium metal anode in liquid electrolytes: challenges and progress, *Adv. Mater.* **30**, 1706375 (2018).

[21] Y. Han, B. Liu, Z. Xiao, W. Zhang, X. Wang, G. Pan, Y. Xia, X. Xia, J. Tu, Interface issues of lithium metal anode for high-energy batteries: Challenges, strategies, and perspectives, *InfoMat.* **3**, 155 (2021).

[22] T. Nishida, K. Nishikawa, M. Rosso, Y. Fukunaka, Optical observation of Li dendrite growth in ionic liquid, *Electrochim. Acta* **100**, 333 (2013).

[23] N. Schweikert, A. Hofmann, M. Schulz, M. Sheuermann, S. T. Boles, T. Hanemann,

H. Hahn, S. Indris, Suppressed lithium dendrite growth in lithium batteries using ionic liquid electrolytes: Investigation by electrochemical impedance spectroscopy, scanning electron microscopy, and in situ ^{7}Li nuclear magnetic resonance spectroscopy, *J. Power Sources* **228**, 237 (2013).

[24] J. Hwang, H. Okada, R. Haraguchi, S. Tawa, K. Matsumoto, R. Hagiwara, Ionic liquid electrolyte for room to intermediate temperature operating Li metal batteries: Dendrite suppression and improved performance, *J. Power Sources* **453**, 227911 (2020).

[25] N. Nishi, Y. Hirano, T. Motokawa, T. Kakiuchi, Ultraslow relaxation of the structure at the ionic liquid|gold electrode interface to a potential step probed by electrochemical surface plasmon resonance measurements: asymmetry of the relaxation time to the potential-step direction, *Phys. Chem. Chem. Phys.* **15**, 11615 (2013).

[26] S. Zhang, N. Nishi, and T. Sakka, Electrochemical surface plasmon resonance measurements of camel-shaped static capacitance and slow dynamics of electric double layer structure at the ionic liquid/electrode interface, *J. Chem. Phys.* **153**, 044707 (2020).

[27] N. Nishi, Y. Ikeda, T. Sakka, Electrochemical surface plasmon resonance as a probe of redox reactions at the ionic liquid|gold interface, *J. Electroanal. Chem*. **817**, 210 (2018).

[28] S. Zhang, T. Sakka, N. Nishi, Slow and fast dynamics at the ionic liquid/gold electrode interface separately probed by electrochemical surface plasmon resonance combined with sequential potential pulse techniques, *J. Electrochem. Soc.* in press. (DOI: 10.1149/1945-7111/ac58c4)

[29] K. Ezawa, N. Nishi, T. Sakka, In-situ electrochemical SPR study of gold surface smoothing by repetitive cathodic deposition and anodic dissolution of copper in an ionic liquid, *J. Electroanal. Chem.* **877**, 114611 (2020).

[30] N. Nishi, K. Ezawa, T. Sakka, In situ surface roughness analysis of electrodeposited Co films in an ionic liquid using electrochemical surface plasmon resonance: Effect of leveling additives, *J. Electrochem. Soc.* **168**, 072505 (2021).

[31] Y. Jin, L. Zhou, J. Yu, J. Liang, W. Cai, H. Zhang, S. Zhu, J. Zhu, In operando plasmonic monitoring of electrochemical evolution of lithium metal, *PNAS* **115**, 11168 (2018).

[32] M. Kitta, K. Murai, K. Yoshii, H. Sano, Electrochemical surface plasmon resonance spectroscopy for investigation of the initial process of lithium metal seposition, *J. Am. Chem. Soc.* **143**, 11160 (2021).

[33] M. Ishikawa, T. Sugimoto, M. Kikuta, E. Ishiko, M. Kono, Pure ionic liquid electrolytes compatible with a graphitized carbon negative electrode in rechargeable lithium-ion batteries, *J. Power Sources* **162**, 658 (2006).

[34] H. Matsumoto, H. Sakaebe, K. Tatsumi, M. Kikuta, E. Ishiko, M. Kono, Fast cycling of Li/$LiCoO_2$ cell with low-viscosity ionic liquids based on bis(fluorosulfonyl)imide $[FSI]^-$, *J. Power Sources* **160**, 1308 (2016).

[35] A. Basile, A. I. Bhatt, A. P. O'Mullane, Stabilizing lithium metal using ionic liquids for long-lived batteries, *Nat. Commun.* **7**, 11794 (2016).

[36] H. Sun, G. Zhu, Y. Zhu, M.-C. Lin, H. Chen, Y.-Y. Li, W. H. Hung, B. Zhou, X. Wang, Y. Bai, M. Gu, C.-L. Huang, H.-C. Tai, X. Xu, M. Angell, J.-J. Shyue, H. Dai, High-safety and high-energy-density lithium metal batteries in a novel ionic-liquid electrolyte, *Adv. Mater.* **32**, 2001741 (2020).

[37] C. J. Jafta, X.-G. Sun, H. Lyu, H. Chen, B. P. Thapaliya, W. T. Heller, M. J. Cuneo, R. T. Mayes, M. P. Paranthaman, S. Dai, C. A. Bridges, Insight into the solid electrolyte interphase formation in bis(fluorosulfonyl)imide based ionic liquid electrolytes, *Adv. Funct. Mater.* **31**, 2008708 (2021).

[38] T. Tamura, T. Hachida, K. Yoshida, N. Tachikawa, K. Dokko, M. Watanabe, New glyme–cyclic imide lithium salt complexes as thermally stable electrolytes for lithium batteries, *J. Power Sources* **195**, 6095 (2010).

[39] K. Yoshida, M. Nakamura, Y. Kazue, N. Tachikawa, S. Tsuzuki, S. Seki, K. Dokko, M. Watanabe, Oxidative-stability enhancement and charge transport mechanism in glyme–lithium salt equimolar complexes, *J. Am. Chem. Soc.* **133**, 13121 (2011).

[40] K. Ueno, J.-W. Park, A. Yamazaki, T. Mandai, N. Tachikawa, K. Dokko, M. Watanabe, Anionic effects on solvate ionic liquid electrolytes in rechargeable lithium–sulfur batteries, *J. Phys. Chem. C* **117**, 20509 (2013).

[41] H. Moon, R. Tatara, T. Mandai, K. Ueno, K. Yoshida, N. Tachikawa, T. Yasuda, K. Dokko, M. Watanabe, Mechanism of Li ion desolvation at the interface of graphite electrode and glyme–Li salt solvate ionic liquids, *J. Phys. Chem. C* **118**, 20246 (2014).

[42] E. Kretschmann, H. Raether, Radiative decay of non radiative surface plasmons excited by light, *Z. Naturforsch., A* **23**, 2135 (1968).

[43] S. Babar, J. H. Weaver, Optical constants of Cu, Ag, and Au revisited, *Appl. Opt.* **54**, 477 (2015).

[44] H. Gerischer, D. Wagner, The underpotential deposition of lithium ions from acetonitrile solutions with small amounts of water, *Ber. Bunsenges. Phys. Chem.* **92**, 1325 (1988).

[45] D. Aurbach, M. Daroux, P. Faguy, E. Yeager, The electrochemistry of noble metal electrodes in aprotic organic solvents containing lithium salts, *J. Electroanal. Chem.* **297**, 225 (1991).

[46] C. A. Berger, M. U. Ceblin, T. Jacob, Lithium deposition from a piperidinium–based ionic liquid: rapping dendrites on the knuckles, *ChemElectroChem* **4**, 261 (2017).

[47] M. Born, E. Wolf, A. B. Bhatia, P. C. Clemmow, D. Gabor, A. R. Stokes, A. M. Taylor, P. A. Wayman, W. L.Wilcock, Principles of optics, *Cambridge University Press* (1999).

[48] D. A. G. Bruggeman, The calculation of various physical constants of heterogeneous substances: I. The dielectric constants and conductivities of mixtures composed of isotropic substances, *Ann. Phys.* **416**, 636 (1935).

[49] S. Zhang, N. Nishi, S. Katakura, T. Sakka, Evaluation of static differential capacitance at the $[C_4mim^+][TFSA^-]$/electrode interface using molecular dynamics simulation combined with electrochemical surface plasmon resonance measurements, *Phys. Chem. Chem. Phys.* **23**, 13905 (2021).

[50] J. C. Slater, Atomic radii in crystals, *J. Chem. Phys.* **41**, 3199 (1964).

[51] Y. Gofer, R. Barbour, Y. Luo, D. Tryk, D. A. Scherson, J. Jayne, G. Chottiner, Underpotential Deposition of Lithium on Polycrystalline Gold from a $LiClO_4$/Poly(ethyleneoxide) Solid Polymer Electrolyte in Ultrahigh Vacuum, *J. Phys. Chem.* **99**, 11739 (1995).

[52] Y. MO, Y. Gofer, E. Hwang, Z. Wang, D. A. Scherson, Simultaneous microgravimetric and optical reflectivity studies of lithium underpotential deposition on Au(111) from propylene carbonate electrolytes, *J. Electroanal. Chem.* **409,** 87 (1996).

[53] P. Bach, I. Valencia-Jaime, U. Rütt, O. Gutowski, A. H. Romero, F. U. Renner, Electrochemical Lithiation Cycles of Gold Anodes Observed by In Situ High-Energy X‑ray Diffraction, *Chem. Mater.* **28**, 2941 (2016).

[54] L. H. S. Gasparotto, N. Borisenko, N. Bocchi, S. Zein El Abedin, F. Endres, In situ STM investigation of the lithium underpotential deposition on Au(111) in the air- and water-stable ionic liquid 1-butyl-1-methylpyrrolidinium bis(trifluoromethylsulfonyl)amide, *Phys. Chem. Chem. Phys.* **11**, 11140 (2009).

[55] K. Motobayashi, K. Matsumoto, S. Tsuzuki, K. Ikeda, Competing characters of Li^+-glyme complex in a solvate ionic liquid: High stability in the bulk and rapid desolvation on an electrode surface, *Electrochem. Sci. Adv.* **e2100150**, 1 (2021).

[56] Z. Yu, C. Fang, J. Huang, B. G. Sumpter, R. Qiao, Solvate ionic liquids at electrified interfaces, *ACS Appl. Mater. Interfaces* **10**, 32151 (2018).

[57] M. Yamagata, N. Nishigaki, S. Nishishita, Y. Matsui, T. Sugimoto, M. Kikuta, T. Higashizaki, M. Kono, M. Ishikawa, Charge–discharge behavior of graphite negative electrodes in bis(fluorosulfonyl)imide-based ionic liquid and structural aspects of their electrode/electrolyte interfaces, *Electrochim. Acta* **110**, 181 (2013).

[58] T. Iwahashi, Y. Miwa, W. Zhou, Y. Sakai, M. Yamagata, M. Ishikawa, D. Kim, Y. Ouchi, IV-SFG studies on the effect of Li^+ in extending the electrochemical window at the Pt|[C_2mim][FSA] interface, *Electrochem. Comm.* **72**, 54 (2016).